6th International Conference on Advances in Experimental Structural Engineering
11th International Workshop on Advanced Smart Materials and Smart Structures Technology
August 1-2, 2015, University of Illinois, Urbana-Champaign, United States

# Experimental Study on Damage Behavior of Steel Plate-Reinforced Concrete Tubes

**H.J. Jiang[1], B. Wang[2], X.L. Lu[3]**

1 *Professor, State Key laboratory of Disaster Reduction in Civil Engineering, Tongji University, Shanghai, China. E-mail: jhj73@tongji.edu.cn*
2 *PhD candidate, State Key laboratory of Disaster Reduction in Civil Engineering, Tongji University, Shanghai, China. E-mail: 2008wangbin@tongji.edu.cn*
3 *Professor, State Key laboratory of Disaster Reduction in Civil Engineering, Tongji University, Shanghai, China. E-mail: lxlst@tongji.edu.cn*

**ABSTRACT**
China Mainland has witnessed a surge in the construction of super tall buildings since the 1990s. The reinforced concrete (RC) tube is one of the predominant structural components popularly used to resist lateral loads in super tall buildings. In recent years steel plate-reinforced concrete (SPRC) tubes have been applied in engineering practice. However, there has been very limited information about the damage behavior of this kind of composite tubes subjected to the earthquake. In this study 1/5-scaled one RC tube and two SPRC tubes with different steel ratio designed according to the current Chinese design code were tested under cyclic lateral loading to assess the seismic performance. The damage characteristics, hysteretic behavior, ductility, strength, shear deformation, crack width, and strain of the specimens were studied. The comparison of the seismic performance between the RC tube and SPRC tube was carried out. The test results show that compared with the RC tube the seismic performance of the SPRC tube is significantly enhanced. The effect of the steel plate ratio on the SPRC tube is not significant.

**KEYWORDS:** *steel plate-reinforced concrete tube, damage behavior, seismic performance, cyclic loading test*

## 1. INTRODUCTION

In China Mainland the RC tube is one of the predominant structural components in super tall buildings used to resist the earthquake. Due to the excessive axial ratio and the demand of high shear strength of RC shear walls in the bottom zone of super tall buildings, the steel plate-reinforced concrete (SPRC) walls or tubes have been developed and applied in engineering practice (Wang, 2012). According to the statistical data, SPRC tubes were adopted in most of the buildings with the height over 400m and the buildings with the height over 200m in the seismic zone with the intensity of 8. However, there has been very limited information about the damage behavior of this kind of composite tube subjected to the earthquake up to now. In this study, according to the current Chinese relevant design code, 1/5-scaled one RC tube and two SPRC tubes with different steel ratio were constructed and tested under lateral cyclic loading to assess the seismic performance. The damage characteristics, hysteretic behavior, ductility, shear deformation and crack width of these specimens were studied.

## 2. EXPERIMENTAL PROGRAM

### 2.1. Description of Test Specimens

The experimental program was designed to investigate SPRC tubes with typical details of those currently used in China. Three 1/5-scaled specimens, one RC tube (numbered as T1) and two SPRC tubes with 4% and 2% steel ratio (numbered as T2 and T3), were designed in line with the current Chinese design code. The dimensions and arrangement of steel bars and steel plated in the specimens are shown in Fig. 2.1. The dimensions and steel reinforcement arrangement for all specimens are identical. The steel plate with the thickness of 4mm and 2mm was embedded in T2 and T3, respectively. The aspect ratio of all specimens is 3.38. The actual strengths of concrete, rebar and steel plate obtained via material property tests are given in Table 2.1 and 2.2, respectively.

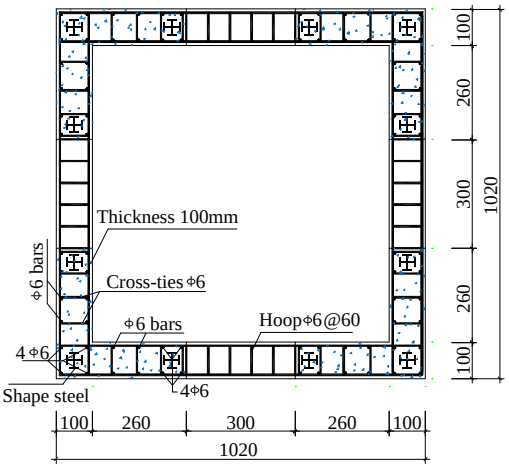


(a) Cross-sectional dimensions of RC tube

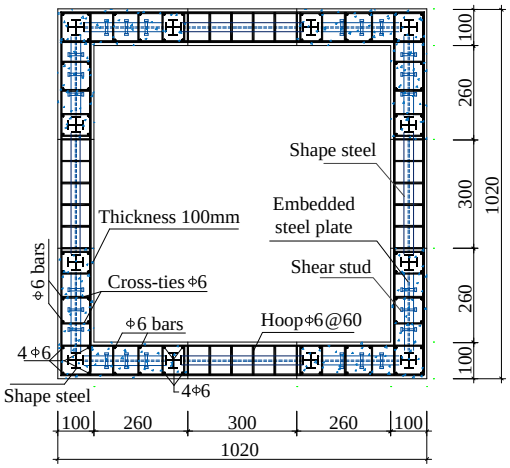


(b) Cross-sectional dimensions of SPRC tubes

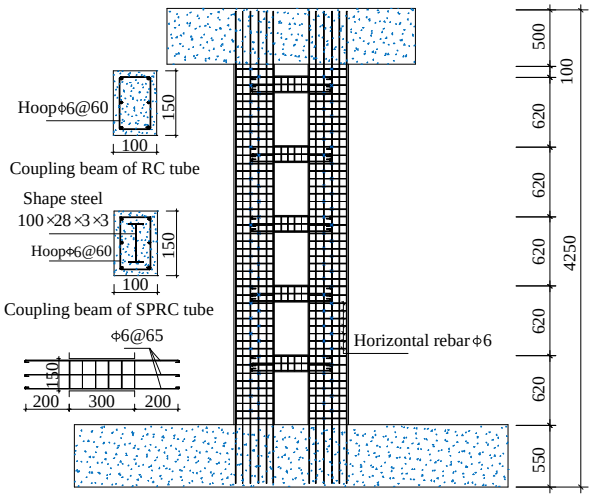


(c) Arrangement of reinforcement

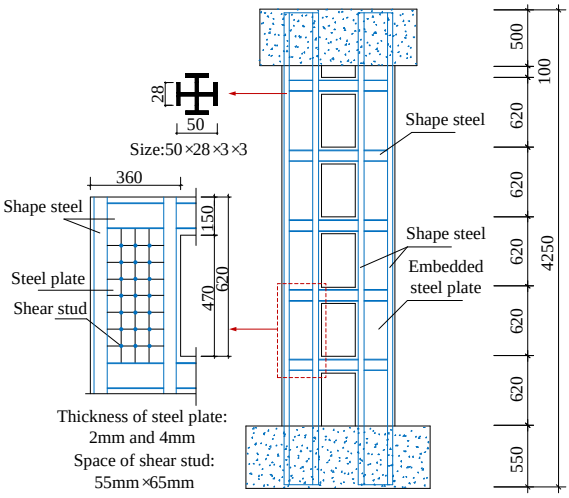


(d) Arrangement of steel plate

Figure 2.1 Configuration of specimens (unit: mm)

Table 2.1 Material properties of concrete (unit: MPa)

| Position | $f_{cu}$ | $E_c$ ($\times 10^4$) |
|---|---|---|
| Pedestal | 45.3 | 3.37 |
| Lower half part of tube | 54.6 | 3.91 |
| Upper half part of tube | 45.1 | 3.37 |
| Loading beam | 44.8 | 3.36 |

Notes: $f_{cu}$ is cubic compressive strength; $E_c$ is elastic modulus.

Table 2.2 Material properties of rebar and steel plate (unit: MPa)

| Types | $f_y$ | $f_u$ | $E_s$ ($\times 10^5$) |
|---|---|---|---|
| Rebar (6mm) | 388 | 494 | 2.08 |
| Steel plate (2mm) | 290 | 408 | 1.98 |
| Steel plate (3mm) | 312 | 414 | 2.02 |
| Steel plate (4mm) | 309 | 445 | 2.09 |

Notes: $f_y$ is yield strength; $f_u$ is ultimate strength; $E_s$ is elastic modulus.

## 2.2. Instrumentation and Test procedures

The test setup is shown in Fig. 2.2. The specimens were extensively instrumented to monitor global responses (e.g., applied lateral load and displacement) as well as local ones (e.g., strain). Linear variable displacement transducers (LVDT) were installed to the monitor rotational, shear, and translational displacement. The shear

deformation was measured through the use of LVDT mounted in the diagonal directions. The lateral displacements at the top and each floor level were measured by the horizontal LVDT. The steel tie bar anchored in the reaction wall and the steel beam pushing against the pedestal were used to restrain the slip of the pedestal. Meanwhile, the LVDT on the pedestal was installed to monitor the slip of the specimen. The strains in the steel bars and steel plate in critical regions were measured by strain gauges. The Digital Image Correlation (DIC) techniques were used to measure the local deformation of the bottom of wall piers and coupling beams.

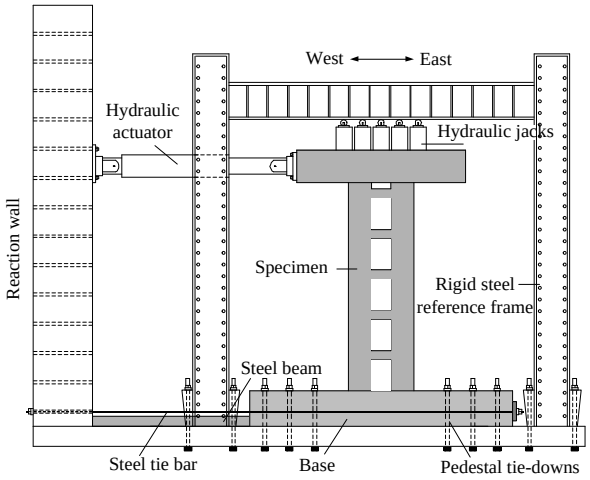


Figure 2.2 Test setup

Firstly the vertical load was exerted on the specimen by hydraulic jacks and kept approximately constant through the whole testing process. The target axial load for all specimens was 1200kN. The actuator attached to the top of the specimen applied the lateral load. Prior to the target displacement of 10mm, the displacement amplitude increment was 2.5mm for one cycle. Then the lateral displacement was applied with the amplitude increment of 10mm for three cycles. Fig. 2.3 illustrates the loading history of all specimens. During the whole test processes, the lateral displacement, force, and the strain were recorded electronically. The maximum crack width was measured at the peak displacement points within each loading cycle. The instrument has the measurement range from 0.04mm to 8mm. For cracks wider than 8mm, the widths were measured by using a steel ruler.

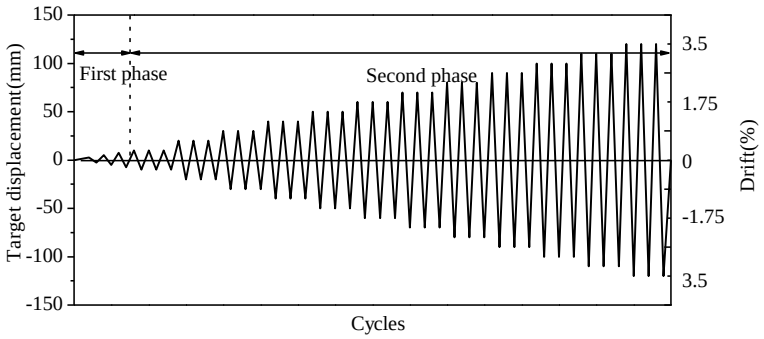


Figure 2.3 Loading history for test

## 3. EXPERIMENTAL RESULTS

The sequences of observed damage are similar for the three specimens. Initial damage was in the form of horizontal cracks appearing at the bottom of wall flange, as shown in Fig. 3.1(a). Subsequently, diagonal cracks on the wall web were observed. With the increase of displacement amplitude, initial crushing and then spalling of the concrete cover at the corner of the coupling beam was detected, as shown in Fig. 3.1(b). New horizontal and diagonal cracks formed and the maximum crack width as well as the maximum residual crack width increased. The crushing and spalling of the concrete cover extended to the edges of the wall piers during the later loading. The significant force in the coupling beam could lead to the fracture of the longitudinal bars, as

shown in Fig. 3.1(c). After the concrete cover completely spalled off and the hoop and longitudinal reinforcement were exposed, the onset of longitudinal bar buckling at the bottom of the boundary element was observed during the subsequent loading cycles, as shown in Fig. 3.1(d). Fracture of the longitudinal bars occurred after bar buckling in specimens T1, T2 and T3, as shown in Fig. 3.1(e). The spalling of the concrete extended from the edges of the wall to the web during the later loading, as shown in Fig. 3.1(f). Because of the lateral restraint effect of the concrete on the steel plate, there is no buckling behavior in the steel plate during the whole loading process, which meets the requirement of structural design.

The behavior of all the specimens was flexure-dominant. The typical development of damage is as follows: the tensile cracking of wall flange, the crack of coupling beam, the diagonal cracks on the wall web, the initial crushing and spalling of the concrete cover at two ends of the coupling beam, the hoop reinforcement exposure of the coupling beam, the crushing and spalling of the concrete cover at the wall pier, fracture of the longitudinal bars or shape steel in the coupling beam, the hoop reinforcement exposure of the wall pier, buckling and fracture of the longitudinal bars or shape steel in the wall pier. It is noted that the top coupling beam and adjacent wall area also had severe damage. This is mainly due to restrain of the loading beam with high stiffness exerting on the deformation of the coupling beam. This kind of damage is not included in this study.

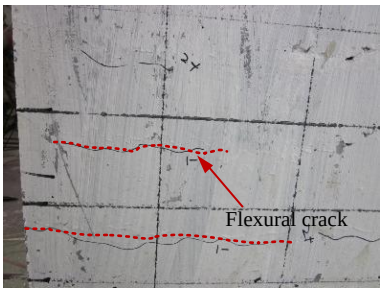


(a) Initial crack pattern (T1) (1/1816)

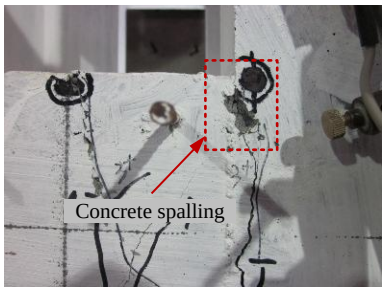


(b) Concrete spalling (T1) (1/94)

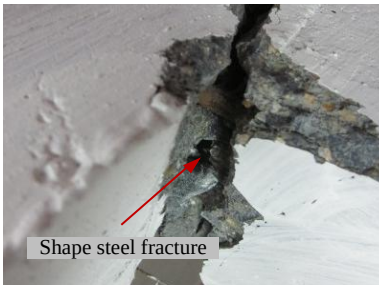


(c) Shape steel fracture (T2) (1/43)

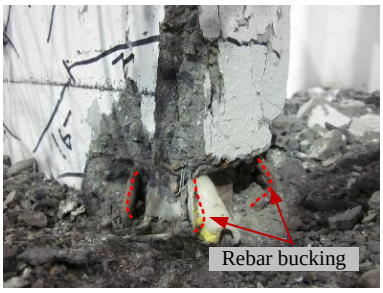


(d) Rebar buckling (T3) (1/31)

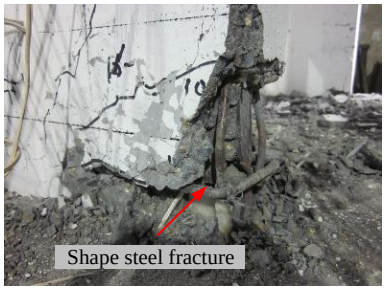


(e) Shape steel fracture (T2) (1/28)

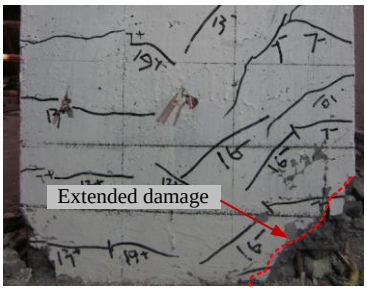


(f) Extended damage (T3) (1/31)

Figure 3.1 Typical damage states of different specimen

Note: The number of the specimen and the drift ratio are shown in brackets.

### 3.1. Hysteretic Behavior

Measured lateral load versus the top displacement (relative displacement between the top of the wall and the pedestal) hysteretic curves for three specimens are shown in Fig. 4.2. Note that the hysteretic curves for all specimens are similar. Specimen T2 and T3 have relatively rounded hysteretic curves than T1 due to the contribution of the embedded steel plates.

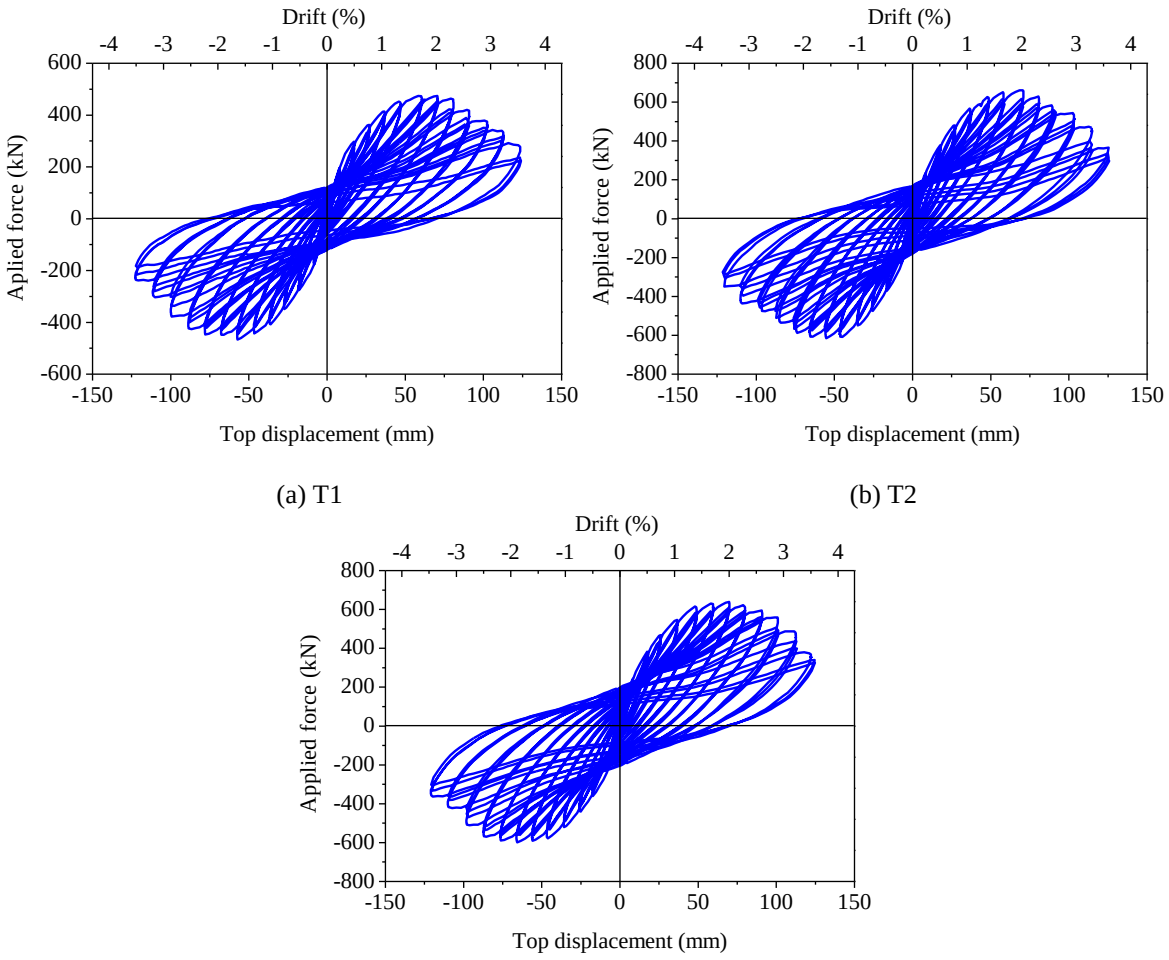


(a) T1 (b) T2

(b) T3

Figure 3.2 Force-displacement hysteretic curves of three specimens

## 3.2. Ductility Evaluation

The ductility is used to measure the ability of a structure or member to maintain the load carrying capacity while deforming beyond yielding. It is generally defined by the displacement ductility coefficient as follows

$$\mu = \frac{|+\Delta_u| + |-\Delta_u|}{|+\Delta_y| + |-\Delta_y|} \tag{3.1}$$

where $\Delta_u$ and $\Delta_y$ are the ultimate and yielding displacement, respectively. In this study, the yielding displacement was determined by the intersection of the horizontal line at maximum force with the straight line passing through the origin and the 75% maximum force point on the envelope curve. The ultimate state was defined by the point on the descending section of the envelope curve with 15% force degradation. Table 3.1 lists the displacement ductility coefficients and the force and the displacement at individual key damage state for all specimens.

From this table it is found that compared with specimen T1, the peak strength of T2 and T3 increases by 39.6% and 34.9%, respectively, which indicates the significant effect of the steel plate on the strength. Compared with the strength of T3 with the steel ratio of 2%, the strength of T2 with the steel ratio of 4% increases by 3.4%. Ductility coefficients of the three specimens are closer and the value of T2 is the smallest. From this point, the ductility of the SPRC tube is not necessarily higher than RC tube.

Table 3.1 Results at key damage state and ductility coefficient

| Specimen | Loading direction | Initial cracking | | Yield | | Peak strength | | Ultimate state | | Ductility |
|---|---|---|---|---|---|---|---|---|---|---|
| | | $F_{cr}$ /kN | $\Delta_{cr}$ /mm | $F_y$ /kN | $\Delta_y$ /mm | $F_{max}$ /kN | $\Delta_{max}$ /mm | $F_u$ /kN | $\Delta_u$ /mm | $\mu$ |
| T1 | Positive | 102.9 | 3.4 | 405.7 | 33.8 | 472.9 | 60.1 | 401.9 | 95.9 | 2.73 |
| | Negative | -48.1 | -1.9 | -405.6 | -36.3 | -460.3 | -57.4 | -391.3 | -96.0 | |
| T2 | Positive | 191.1 | 6.1 | 582.3 | 38.1 | 660.3 | 70.5 | 561.3 | 99.5 | 2.67 |
| | Negative | -126.8 | -3.4 | -533.3 | -32.5 | -615.2 | -55.3 | -522.9 | -88.8 | |
| T3 | Positive | 186.1 | 5.7 | 548.5 | 36.3 | 638.4 | 69.9 | 542.6 | 103.4 | 2.75 |
| | Negative | -113.9 | -3.5 | -534.7 | -36.7 | -599.3 | -65.7 | -509.4 | -97.9 | |

### 3.3. Shear Deformation

The shear force-shear deformation hysteretic curves for the bottom storey of each specimen are shown in Fig. 3.3. It is found that the shear deformation of T2 and T3 are significantly less than that measured in specimen T1. The shear force-shear deformation curve of T1 shows the pinch effect. On the contrary, T2 and T3 have the relative rounded hysteretic curves, owing to the contribution of embedded steel plate.

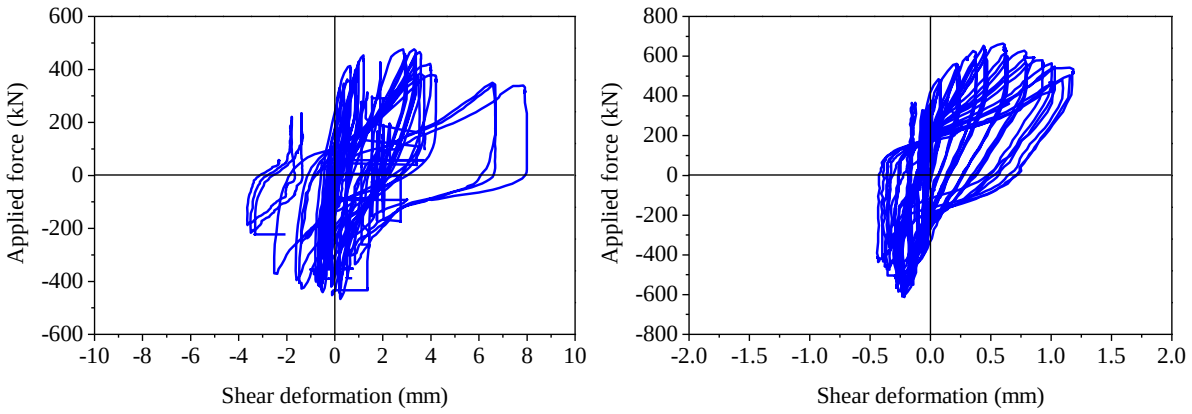


(a) T1 (b) T2

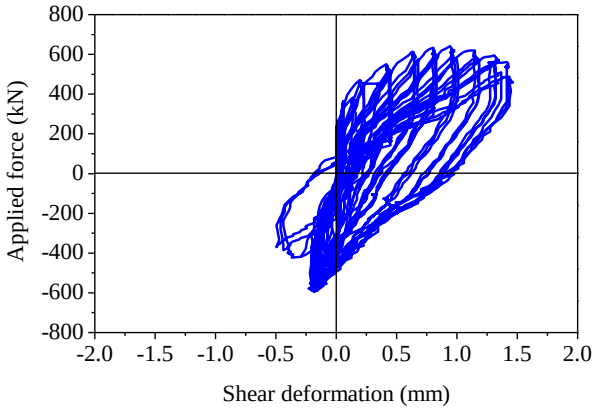


(b) T3

Figure 3.3 Shear force-shear deformation hysteretic curves of three specimens

### 3.4. Crack Characteristics

The crack width is considered as an important index for evaluating the damage level of structural components under earthquakes. The maximum crack width $w_m$ of the wall piers and the coupling beam is shown in Fig. 3.4. Note that in a global sense the maximum crack width increases monotonically with the increase of drift level in all specimens. The steel plate in the wall pies can constrain the crack development and the crack widths of T2 and T3 are smaller than that of T1. Nevertheless, the fracture of shape steel and longitudinal bar in the coupling beam will result in significantly increased crack width in SPRC tubes.

It is found that the coupling beam is the first seismic defense in coupled shear walls or tubes. The crack width of the wall piers is far less than that of the coupling beam. The value of crack width of wall piers in coupled shear walls or tubes is quite different from the value of the isolated wall (Jiang, 2013).

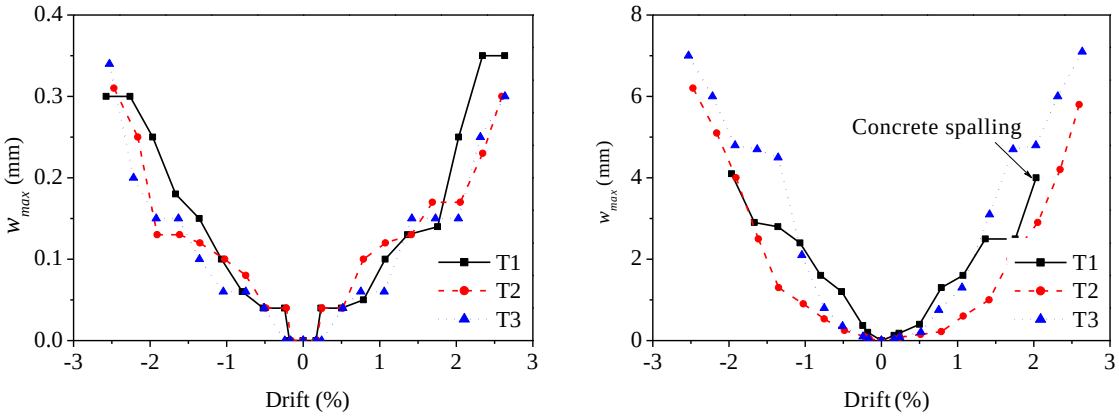


(a) Wall pier (b) Coupling beam

Figure 3.4 Maximum crack width versus drift ratio relationship

## 3.5. Strain Measurement by DIC Technique

The theory of Digital Image Correlation (DIC) has been described in detail by several researchers (Sutton, 2009). DIC has been commonly used for small-scale mechanical device and some material tests, but has only recently been extended to large civil structures. It allows measurement of large deformations and strains, far beyond the elastic limit of the material. The experiment on Specimen T1 was divided into two phases, and the strain analysis was only carried out the first phase. To get the comparative results, the unified target drift of 1/125 was taken for the three specimens. The longitudinal strain and maximum principal strain of wall piers and the coupling beam are shown in Fig. 3.5. Compared with T1, the longitudinal strain of T2 and T3 decreased considerably due to the effect of embedded steel plate. This also explains the improvement of steel plate to the axial compression effect. Similarly, the maximum principal strains of T2 and T3 are also smaller than the that of T1.

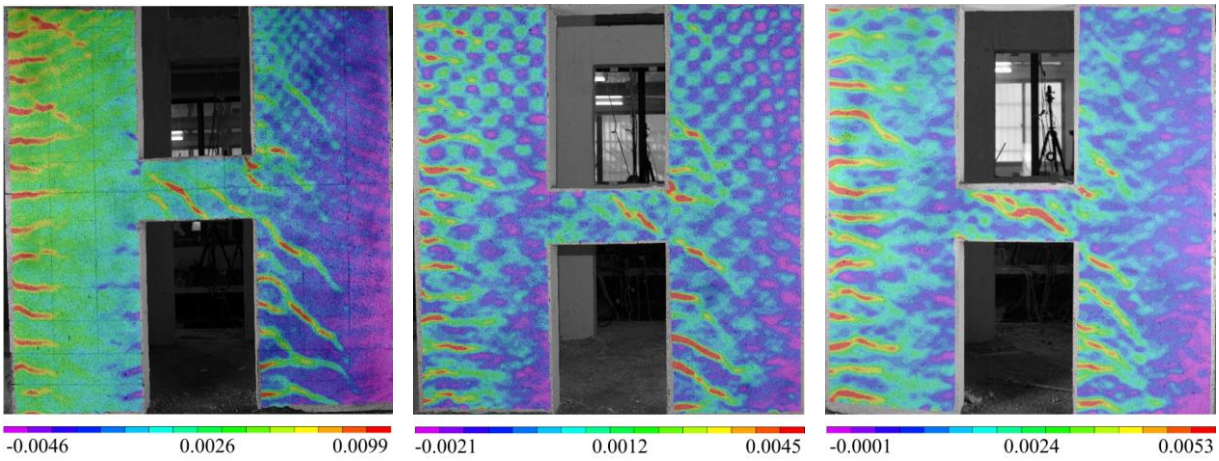


(a) Longitudinal strain of T1 (b) Longitudinal strain of T2 (c) Longitudinal strain of T3

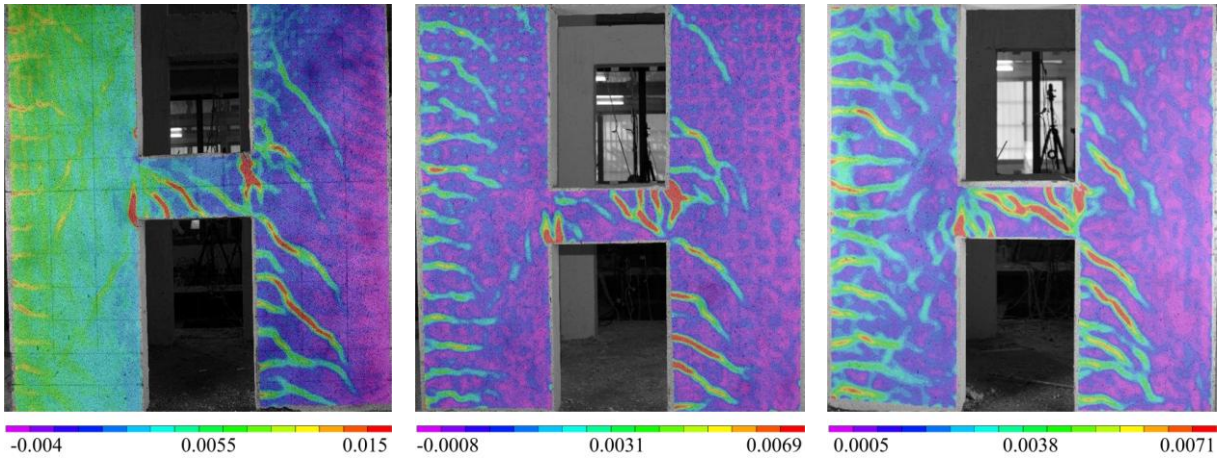


(d) Maximum principal strain of T1 (e) Maximum principal strain of T2 (f) Maximum principal strain of T3

Figure 3.5 Strain profiles of wall piers and coupling beam at drift ratio of 1/125

## 4. CONCLUSIONS

1/5-scaled one RC tube and two SPRC tubes with 4% and 2% steel ratio were tested under lateral cyclic loading to assess the seismic performance. The damage characteristics, hysteretic behavior, ductility, shear deformation and crack width of the specimens were studied. The following conclusions can be drawn from the test results:

(1) The sequences of observed damage are similar for all specimens. The behavior of all specimens is flexure-control. Because of the lateral restraint effect of the concrete on the steel plate, there is no buckling in the steel plate during the whole loading process, which meets the requirement of structural design.

(2) For the SPRC tube, compared with the RC tube, the shear deformation decreases, the lateral load carrying capacity increases, the maximum width of the crack in the wall pier decrease, and the force-displacement hysteretic curves are more rounded.

(3) Owing to the contribution of the embedded steel plate, compared with the RC tube, the seismic performance of SPRC tube is significantly improved.

(4) The effect of steel plate ratio on the SPRC is not significant.

**AKCNOWLEDGEMENT**

The financial support from the National Natural Science Foundation of China under grant Nos. 51478354 and 91315301-4 is gratefully acknowledged.

**REFERENCES**

1. Jiang, H. J., Wang, B, and Lu, X. L. (2013). Experimental Study on Damage Behavior of Reinforced Concrete Shear Walls Subjected to Cyclic Loads. *Journal of Earthquake Engineering*. **17:7**, 958-971.
2. Sutton, M. A., Orteu, J. J., and Schreier, H. (2009). Image Correlation for Shape, Motion and Deformation Measurements: Basic Concepts, Theory and Applications. Springer Science & Business Media.
3. Wang, B., Jiang, H. J., Lu, X. L. (2012). Seismic Performance of Steel Plate-Reinforced Concrete Composite Shear Wall. *The 15th World Conference on Earthquake Engineering*. Lisboa, Portugal. Paper number: 1232.